SCIENTIFIC REP✺RTS

Magnetic MoS$_2$ pizzas and sandwiches with Mn$_n$ (n = 1–4) cluster toppings and fillings: A first-principles investigation

Meng Zhang[1], Zhongjia Huang[2], Xiao Wang[1], Hongyu Zhang[1], Taohai Li[3], Zhaolong Wu[1], Youhua Luo[1] & Wei Cao[4]

The inorganic layered crystal (ILC) MoS$_2$ in low dimensions is considered as one of the most promising and efficient semiconductors. To enable the magnetism and keep intrinsic crystal structures, we carried out a first-principles study of the magnetic and semiconductive monolayer MoS$_2$ adsorbed with the Mn$_n$ (n = 1–4) clusters, and bilayer MoS$_2$ intercalated with the same clusters. Geometric optimizations of the Mn$_n$@MoS$_2$ systems show the complexes prefer to have Mn$_n$@MoS$_2$(M) pizza and Mn$_n$@MoS$_2$(B) sandwich forms in the mono- and bi-layered cases, respectively. Introductions of the clusters will enhance complex stabilities, while bonds and charge transfers are found between external Mn clusters and the S atoms in the hosts. The pizzas have medium magnetic moments of 3, 6, 9, 4 μ_B and sandwiches of 3, 2, 3, 2 μ_B following the manganese numbers. The pizzas and sandwiches are semiconductors, but with narrower bandgaps compared to their corresponding pristine hosts. Direct bandgaps were found in the Mn$_n$@MoS$_2$(M) (n = 1,4) pizzas, and excitingly in the Mn$_1$@MoS$_2$(B) sandwich. Combining functional clusters to the layered hosts, the present work shows a novel material manipulation strategy to boost semiconductive ILCs applications in magnetics.

Since a pioneering (re)discovery of the monolayer graphene[1,2], enormous researches have been focused on layered crystals during the past decades[3]. Benefiting from covalence bonds in layers and van der Waals forces among layers, complex structures are easily manipulated in order to reach different application purposes. In contrast to the semimetallic pristine graphene, most of the inorganic layered crystals (ILCs) have non-zero bandgaps. Such semiconducting properties are essential in semiconductor industry. Various species from the nitrides and group VI metal compounds[4] enrich the library of the ILCs. Among them, the MoS$_2$ is a conventional lubricant[5] and catalyst for hydrogen evolution[6,7]. When lowering the MoS$_2$ dimensions, a transition of indirect to direct band occurs, leading to the boosting of photoluminescence[8,9]. Recent investigations of the materials in low dimensions showed that it is advanced in high efficient transistors[10], photoelectronic devices[11], and electrocatalysis[12]. To improve the performances of the MoS$_2$-based devices, molecular modulation and engineering are proposed and many of works are in progresses[13,14]. Ideally speaking, the ILC materials can be piled up to 3D forms, with each 2D layer consisting of enough functional units such as doped atoms or clusters[4]. So is the few-layer MoS$_2$, which has potentials in various applications and was reported as a key material in high mobility and low power transistors[10,15].

Pursuing semiconductors with high performances has always been within the focuses of materials sciences. Due to possible manipulations of electron spins and carrier intensities[16], dilute magnetic semiconductors (DMSs) have been one of the key targets within such an issue. Similar to the hosting merits from the transition metal (TM) oxides (say the ZnO)[17], the structural uniqueness of ILCs makes such layered groups as new candidate matrixes in the magnetic semiconductors. The 2D DMS systems have been explored in monolayer MoS$_2$ e.g., by substituting Mo ions with 3d TMs[18,19] or 4d TMs[20]. The doping routes in the ILCs are, nevertheless, not an easy task in

[1]Department of Physics, East China University of Science and Technology, Shanghai 200237, China. [2]School of Mechanical and Automotive Engineering, Anhui Polytechnic University, Wuhu 241000, China. [3]College of Chemistry, Key Lab of Environment Friendly Chemistry and Application in Ministry of Education, Xiangtan University, Xiangtan, 411105, China. [4]Research Centre for Molecular Materials, University of Oulu, P.O. Box 3000, FIN-90014, Finland. Correspondence and requests for materials should be addressed to Y.L. (email: yhluo@ecust.edu.cn) or W.C. (email: wei.cao@oulu.fi)
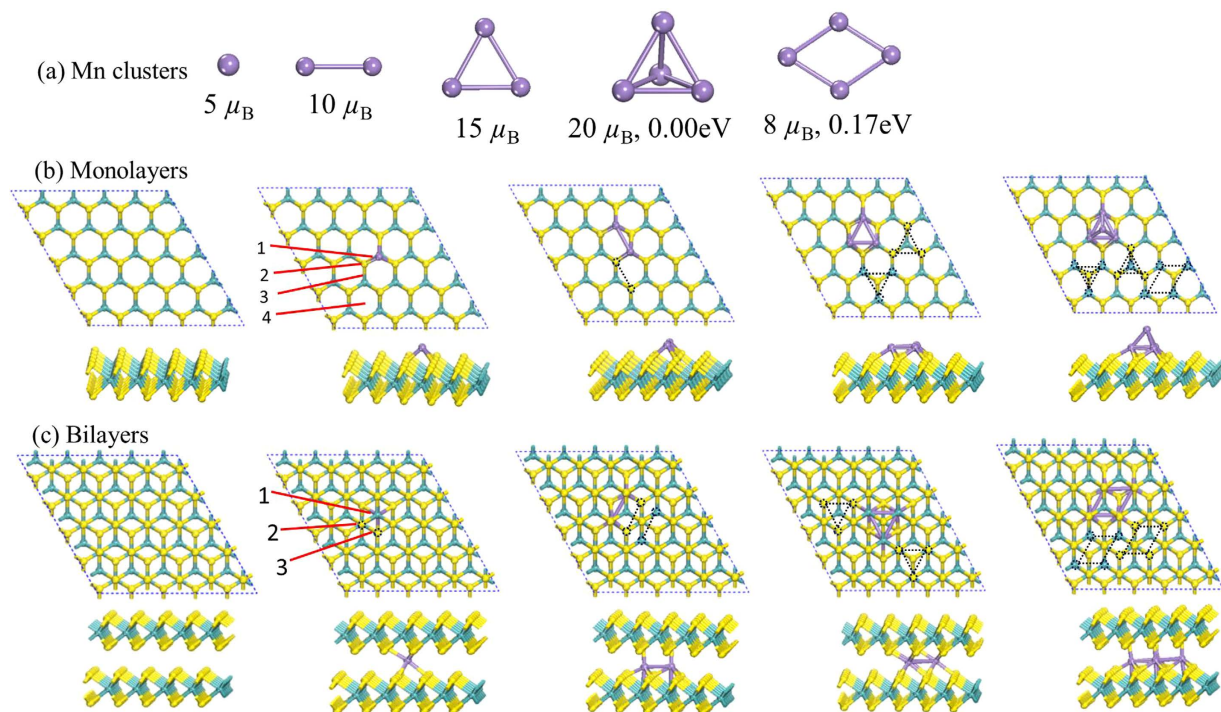
Figure 1. Optimized geometric structures. (**a**) The Mn_n (n = 1–4) clusters, (**b**) the Mn_n clusters adsorbed on monolayer, and (**c**) bilayer MoS_2 from the top view (up) and the side view (below). The blue, yellow and purple spheres represent the Mo, S and Mn atoms, respectively. Possible adsorption sites are labelled in numbers in (**b,c**). The dash-dot ball and line refer to metastable positional alignments of the Mn_n clusters adsorbed on the MoS_2 host upon geometry optimization.

experiments[21]. Alternatives were suggested to replace both Mo and neighboring S atoms with the FeX_6 (X = S, C, N, O, F) clusters[22], or a wetting deposition of the Co layer onto monolayer MoS_2[23]. Brewing magnetism into double- or few-layered MoS_2 are rather scarcely reported, despite of the magnification of efficiencies in the 3D piled-up electronics[4]. In a latest work, the Fe doped double layered MoS_2 was predicted to enhance the host stabilities as well as to magnetically exchange coupling between the host and dopants[24]. However, doping or growing dynamics of such hetero functional units normally debuts from a fast nucleation of the metallic ions[25,26], resulting in rather small clusters or nanoparticles on the layered crystal surfaces or possibly among the layers[27–29]. Indeed, in addition to clusters' inimitable properties[30,31], combining clusters with the monolayer graphene was predicted to increase the magnetic moment of the cluster[32–34]. Furthermore, the intercalated water molecules between graphene interlayers were observed experimentally and very unique properties have been revealed recently[35]. Thus, in an analogy to routes of clusters anchoring on the graphene, using the clusters as dopants onto or among the ILCs may offer another effective route to tailor the ILCs properties.

In this article, we reported on a first-principles prediction of magnetic monolayer MoS_2 'pizzas' with Mn_n (n = 1–4) 'toppings', and bilayer MoS_2 'sandwiches' with Mn_n (n = 1–4) clusters 'fillings'. The manganese clusters were selected as the start clusters due to their magnetic robustness[36], size-dependent magnetism[37], as well as easier adsorptions on layered structures[38]. Hosts of the clusters were extended from monolayer MoS_2 'crust' to the bilayer 'bread slices'. To keep the intrinsic layered structures and prevent introducing defects, the clusters were placed and adsorbed on the top or between the layers. We investigated magnetic properties and electronic structures of the cluster adsorbed mono- and bi-layers. Bonding mechanisms within Mn clusters, and between clusters and ILC hosts were studied. In addition to possible variations of magnetic moments by changing the cluster sizes, we also found that introductions of the clusters into the ILC systems will facilitate system stabilities, and operate band types.

Results

Geometric structures of the complexes. Investigations of the doped system's properties debut from the geometric structures. The free Mn_n clusters were firstly studied to give basic knowledge of the 'toppings' or 'fillings' onto or into the crusts or bread slices. More than 60 initial Mn_n structures were collected for further DFT optimization. Optimized clusters geometries were depicted in Fig. 1a. Detailed structural parameters for other low-lying isomers are provided in the Supplementary Information (SI). The Mn_n clusters evolved from 0D to 2D forms when n was tuned from 1 to 3. However, in the case of n = 4, the 3D tetrahedron cluster was found as the most stable isomer, followed by a rhombus with a relative energy of 0.17 eV higher. Our results of free Mn clusters are in agreement with the previous DFT calculations[39–41].

Layer Number	System Name	Optimized bond distance (Å)			E_{ad} (eV)
		d_{Mn-Mn}	nearest d_{Mn-S}	farthest d_{Mo-S}	
0	Mn$_2$ cluster	2.633	—	—	—
	Mn$_3$ cluster	2.791	—	—	—
	Mn$_4$ cluster	2.764	—	—	—
1	pristine	—	—	2.437	—
	Mn$_1$@MoS$_2$	—	2.207	2.610	−1.631
	Mn$_2$@MoS$_2$	2.877	2.116	2.654	−2.897
	Mn$_3$@MoS$_2$	2.720	2.181	2.556	−4.207
	Mn$_4$@MoS$_2$	2.631	2.206	2.531	−4.725
2	pristine	—	—	2.432	—
	Mn@MoS$_2$	—	2.327	2.472	−2.791
	Mn$_2$@MoS$_2$	2.917	2.086	2.578	−5.013
	Mn$_3$@MoS$_2$	2.956	2.238	2.457	−6.527
	Mn$_4$@MoS$_2$	2.940	2.087	2.469	−8.787

Table 1. Adsorption energies E_{ad} (in eV) and bond lengths d (in Å) of the Mn$_n$ (n = 1–4) clusters adsorbed on the monolayer and bilayer MoS$_2$. The MoS$_2$ layer number was set 0 for the free manganese clusters.

From the hosts' side, the 5 × 5 supercells of single- and two-layer MoS$_2$ were firstly relaxed and the optimized results were shown on the left row in Fig. 1b,c. The lattice constants are 3.21 and 3.20 Å for the monolayer and bilayer MoS$_2$, respectively, in good agreements with other density functional theory (DFT) calculations[42]. In general, the energy and magnetic properties of the Mn$_n$@MoS$_2$ systems are sensitive to coordination and contact positions of the Mn$_n$ clusters with respect to the ILC hosts. In what follows, we name the systems of Mn$_n$@MoS$_2$(M) for the Mn$_n$ cluster doped Monolayer complexes, and Mn$_n$@MoS$_2$(B) for the Bilayer ones. After a full optimization of all possible motifs including magnetic order effects, it is found that the Mn$_n$@MoS$_2$(M) prefer pizza structures. Manganese clusters maintain their initial geometries after being adsorbed on the MoS$_2$ monolayer. However, the Mn clusters evolve to a parallel layer motif when intercalated in the bilayers. The Mn$_n$@MoS$_2$(B) have sandwich structures with the maximal coordination numbers to expand the interactions between the Mn$_n$ clusters and two layers of the MoS$_2$.

Geometric arrangements of the Mn$_n$ clusters and their hosts were studied in details. For the Mn$_n$@MoS$_2$(M), the most stable adsorption sites of the Mn atoms are right above the Mo atom (numbered 1 in Fig. 1b) from the top view. Other possible adsorption sites on-top S atom, bridge and face as labelled 2, 3, and 4 in Fig. 1b are energetically unfavorable. Our optimizations show that each Mn adatom is bonded to three S atoms at the monolayer MoS$_2$ site. For the Mn$_4$@MoS$_2$(M), the most stable structure is constructed by the tetrahedron Mn$_4$ cluster whose triangular face lays on the MoS$_2$ host. The rhombic structure with four Mn atoms tiled above the Mo site is less stable with higher energy as shown in Fig. 1b. On the contrary, the structure of the three-dimensional tetrahedron Mn$_4$ cluster sandwiched between two layers of the MoS$_2$ is unstable according to our calculation. In the figures, the dash-dot balls and lines refer to metastable positions of the Mn$_n$ clusters on the monolayer MoS$_2$. However, in the case of inserting Mn$_n$ to bilayer MoS$_2$ systems, the lowest energy structures exhibit odd-even alternations with the number of the Mn atoms. One Mn atom laying under the Mo atom (labelled 1 in Fig. 1c) is the lowest energy structures of odd number n with each adatom Mn bonding six S atoms in the bilayer MoS$_2$, while the Mn atoms preferring to be under the S atom (featured 2 in Fig. 1c) and forming the most stable Mn$_n$@MoS$_2$(B) (n = 2,4) complexes. In this case of evenly numbered n, each Mn atom is bonded to four host S atoms and one Mo atom as Fig. 1c shows.

Bonding scheme and stability. Table 1 gives bond lengths of the Mn$_n$ clusters adsorbed on the monolayer and bilayer MoS$_2$ at the most stable adsorption sites. Two kinds of hosting atoms are classified: participators with whom dopants are bonded, and spectators where no additional bonding are formed. The MoS$_2$ honeycomb structures remain unchanged after absorptions of the Mn$_n$ clusters. Very slight lattice distortions are found at the participator area near the Mn$_n$ clusters. From Table 1, it can be seen that the distances of the d_{S-Mo} between the participator atoms of the MoS$_2$ became larger than those of the pristine MoS$_2$ in both the 'pizza' and 'sandwich' cases. These participator S atoms interact with the impurity Mn$_n$ clusters, weakening bonding between the S and Mo atoms. On the contrary, the bond length of spectator atoms is the same as the one of the pristine MoS$_2$. The Mn-Mn bond lengths in 'pizzas' and 'sandwiches', except for the Mn$_3$@MoS$_2$(M) and Mn$_4$@MoS$_2$(M), are notably larger than those in the free Mn$_n$ clusters, also indicating a covalent-bond interaction between the Mn and S atoms. The Mn-Mo bond lengths in Mn$_2$@MoS$_2$(B) and Mn$_4$@MoS$_2$(B) are 2.762 and 2.800 Å, respectively. Notably, values of the farthest d_{Mo-S} in Mn$_n$@MoS$_2$(B) oscillate with the Mn numbers. The oscillating trend pervades to electronic and magnetic properties of the Mn$_n$@MoS$_2$ (B) sandwiches in the follow discussion.

The adsorption energies E_{ad} of the Mn$_n$ clusters adsorbed on the ILC hosts were computed as follows.

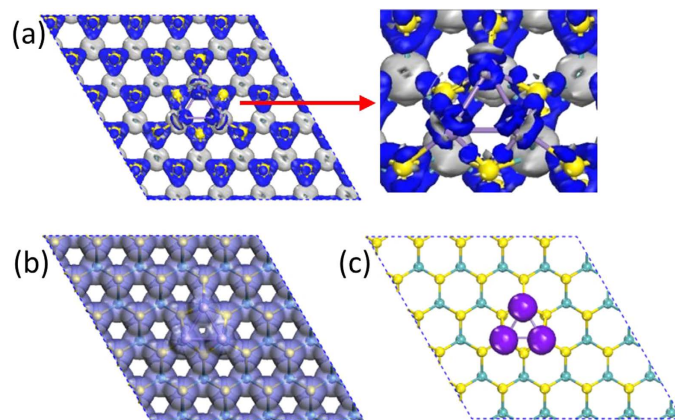$$E_{ad} = E_{total}(Mn_n@MoS_2) - [E_{total}(MoS_2) + E_{total}(Mn_n)], \qquad (1)$$

Figure 2. Electron densities of the Mn₃@MoS₂(M) complex. (**a**) The deformation electron density (DED). Charge accumulations are obvious in blue regions and depletions in silvery regions. (**b**) Total electron density. (**c**) The net spin electron density. The surface isovalue for electron density is 0.04 e/Å³.

where $E_{total}(Mn_n@MoS_2)$ and $E_{total}(MoS_2)$ represent the total energies of the lowest-energy structures of the adsorbates and pristine MoS_2, respectively, and $E_{total}(Mn_n)$ is the energy of the individual Mn_n clusters. All adsorption energies are found largely below zero (see Table 1), indicating stability of MoS_2 after the introductions of the Mn_n clusters. Obviously, the absolute value of E_{ad} increases with the numbers of the Mn atoms due to the increase of the covalent-bond interaction between the Mn and S atoms. To have a better view of the interactions between the Mn_n clusters and MoS_2 layers, the deformation electron density (DED) of the $Mn_3@MoS_2(M)$ for the lowest-energy structures was plotted in Fig. 2a as an example. The DED is defined as the total charge density of a system with the density of the isolated atoms subtracted. The blue and silvery area indicate electron accumulation and depletion when atoms forming the $Mn_3@MoS_2(M)$. When the Mn_3 cluster is adsorbed on the MoS_2 slab, the DED distributes not only surrounding the Mo and S atoms in the host MoS_2 but also remarkably at the intervals between the Mn and S atoms and the guest Mn clusters (see Fig. 2a). Featuring covalent characters of the S-Mn bonds, the DED identifies strong interactions between the Mn and S in the $Mn_n@MoS_2(M\&B)$ and high stability of the structure due to such interactions.

Magnetic properties. The lowest-spin arrangements of individual clusters are all ferromagnetic from our present calculations. Magnetic moments of the Mn_n (n = 1–4) clusters are 5, 10, 15, and 20 μ_B, respectively, in agreement with previous studies[40–42]. It is important to understand the host influence on the magnetic orders of the magnetic guests. For this purpose, we optimized all magnetic spin states of the lowest-energy structures of the 'pizzas' and 'sandwiches' from Fig. 1b,c. Table 2 gives the relative energies with respect to the most stable spin states of the Mn_n clusters adsorbed on the ILC hosts at the lowest energy adsorption sites. Results show that magnetic moments of the impurity Mn_n clusters are not quenched by the nonmagnetic host MoS_2 substrate. The energetic magnetic spin state displays ferrimagnetic properties when ferromagnetic Mn clusters adsorbed on the MoS_2. The $Mn_n@MoS_2(M)$ pizzas prefer to have medium magnetic moments of 3, 6, 9, and 4 μ_B in comparison with their corresponding free Mn_n clusters (5, 10, 15, 20 μ_B). The $Mn_n@MoS_2(B)$ sandwiches exhibit favorable oscillatory behavior with relatively smaller magnetic moments of 3, 2, 3, and 2 μ_B. To reveal detailed contributions from each Mn atom in the 'topping' or 'fillings', we also studied the local spin state on the Mn atom of the $Mn_n@MoS_2$ (M&B) systems. Their magnetic moments are listed in Table S1 (see details in SI). The Mn atoms in $Mn_n@MoS_2(M)$ pizzas are in ferromagnetic states except for theses of the $Mn_4@MoS_2(M)$. On the $Mn_4@MoS_2(M)$ pizza, three tiled Mn atoms have "spin-up" (majority) magnetic moments and one top Mn atom has "spin-down" (minority) magnetic moments. While in the $Mn_n@MoS_2(B)$ sandwiches, the Mn atoms display ferrimagnetic order as shown in Table S1. Thus the guest Mn_n clusters may serve as an ideal system to tailor magnetic properties when introduced on or between the MoS_2 'crust' or 'bread slices'. Continued experimental and theoretical studies of similar TM clusters adsorbed on MoS_2 systems may lead to discoveries of new families of dilute magnetic semiconductors with tunable magnetic properties.

It should be noted that the magnetic properties of the Mn_7 cluster absorbed on graphene exhibits a magnetic moment of 6.3 μ_B per cell as given by first-principles calculations[32]. This value is 1.3 μ_B larger than 5.0 μ_B in an isolated Mn_7 cluster. In the case of Mn doped MoS_2 studied through a combination of DFT calculations and Monte Carlo simulations, the overall magnetic moment of the supercell is 1 μ_B corresponding to the single excess d electron provided by the Mn atom[43]. On the other hand, magnetic properties of nonmetal atoms adsorbed MoS_2 monolayers were also investigated by first-principles calculations. The total magnetic moments of H-,B-, C-, N-, and F-adsorbed MoS_2 monolayers were found 1, 1, 2, 1, and 1 μ_B, respectively[44]. The magnetic motifs of all these three cases are different from that of the $Mn_n@MoS_2$ 'pizzas' and 'sandwiches' studied here. By comparing the magnetic properties between other cases and this work, more insights may be provided into the effect of the impurities types employed on a nonmagnetic layer host.

Mulliken population analysis shows that the total magnetic moment of the clusters is mainly localized in the Mn atoms as tabulated in Table 3. A small amount of magnetic moment is found in host Mo and S atoms. To

Monolayer	$M(\mu_B)$	ΔE(eV)	Bilayer	$M(\mu_B)$	ΔE(eV)
Mn@MoS$_2$	1	0.62	Mn@MoS$_2$	1	0.25
	3	0		3	0
	5	0.23		5	0.15
Mn$_2$@MoS$_2$	0	—	Mn$_2$@MoS$_2$	0	0.06
	2	0.09		2	0
	4	0.31		4	0.16
	6	0		6	0.15
	8	0.07		8	0.63
	10	0.32		10	1.29
Mn$_3$@MoS$_2$	1	0.21	Mn$_3$@MoS$_2$	1	0.09
	3	0.31		3	0
	5	0.93		5	0.13
	7	0.42		7	0.18
	9	0		9	0.1
	11	0.02		11	0.21
	13	0.49		13	0.36
	15	0.89		15	0.55
Mn$_4$@MoS$_2$	0	0.24	Mn$_4$@MoS$_2$	0	0.05
	2	0.07		2	0
	4	0		4	0.26
	6	0.28		6	0.36
	8	0.31		8	0.55
	10	0.16		10	—
	12	0.04		12	0.88
	14	0.23		14	1.39
	16	0.66		16	1.95
	18	1.03		18	2.59
	20	1.38		20	—

Table 2. Magnetic moments M (μ_B) of the Mn$_n$ cluster adsorbed MoS$_2$ complexes. Metastable isomers of other magnetic moments have different relative energies of ΔE (in eV) with respect to the most stable ones. The hyphen (—) means the structure is not converged during the optimization.

System	magnetic moment (μ_B)				charge	
	Mn	Mo	S	total	Mn	bandgap
pristine	—	0	0	0	—	1.687
Mn@MoS$_2$(M)	3.26	−0.132	−0.128	3	0.053	0.463
Mn$_2$@MoS$_2$(M)	6.706	−0.502	−0.204	6	−0.07	0.327
Mn$_3$@MoS$_2$(M)	9.578	−0.362	−0.216	9	−0.175	0.245
Mn$_4$@MoS$_2$(M)	4.579	−0.51	−0.069	4	−0.215	0.137
pristine	—	0	0	0	—	1.144
Mn@MoS$_2$(B)	2.881	0.027	0.092	3	−0.32	0.272
Mn$_2$@MoS$_2$(B)	2.042	−0.016	−0.026	2	−0.771	0.490
Mn$_3$@MoS$_2$(B)	3.195	−0.224	0.029	3	−0.808	0.245
Mn$_4$@MoS$_2$(B)	1.953	0.147	−0.1	2	−1.715	0.276

Table 3. Charge transfer and local magnetic moments of the Mn$_n$ cluster adsorbed MoS$_2$ complexes. Mulliken Charge (in au) were counted on the Mn atoms, local magnetic moment (in μ_B) on the guest Mn clusters, host Mo and S atoms. Total magnetic moment (in μ_B) and bandgap (in eV) of the Mn$_n$ clusters absorbed on monolayer and bilayer MoS$_2$ per supercell were also tabulated herein.

visualize the spin distribution of the Mn$_n$@MoS$_2$(M) 'pizza', the isosurface spin density of the 'pizza' was plotted in Fig. 2. It can be seen from Fig. 2b,c that although the total charge density is extended over the whole Mn$_3$@MoS$_2$(M), the spin density is almost entirely located on the Mn$_3$ cluster site, resulting in a robust magnetic moment of 9 μ_B for the Mn$_3$@MoS$_2$(M).

Electronic structures. The band structures of the Mn$_n$@MoS$_2$(M&B) complexes were plotted in Fig. 3 for the lowest-energy structures. These from the pristine monolayer and bilayer MoS$_2$ were also given for comparison
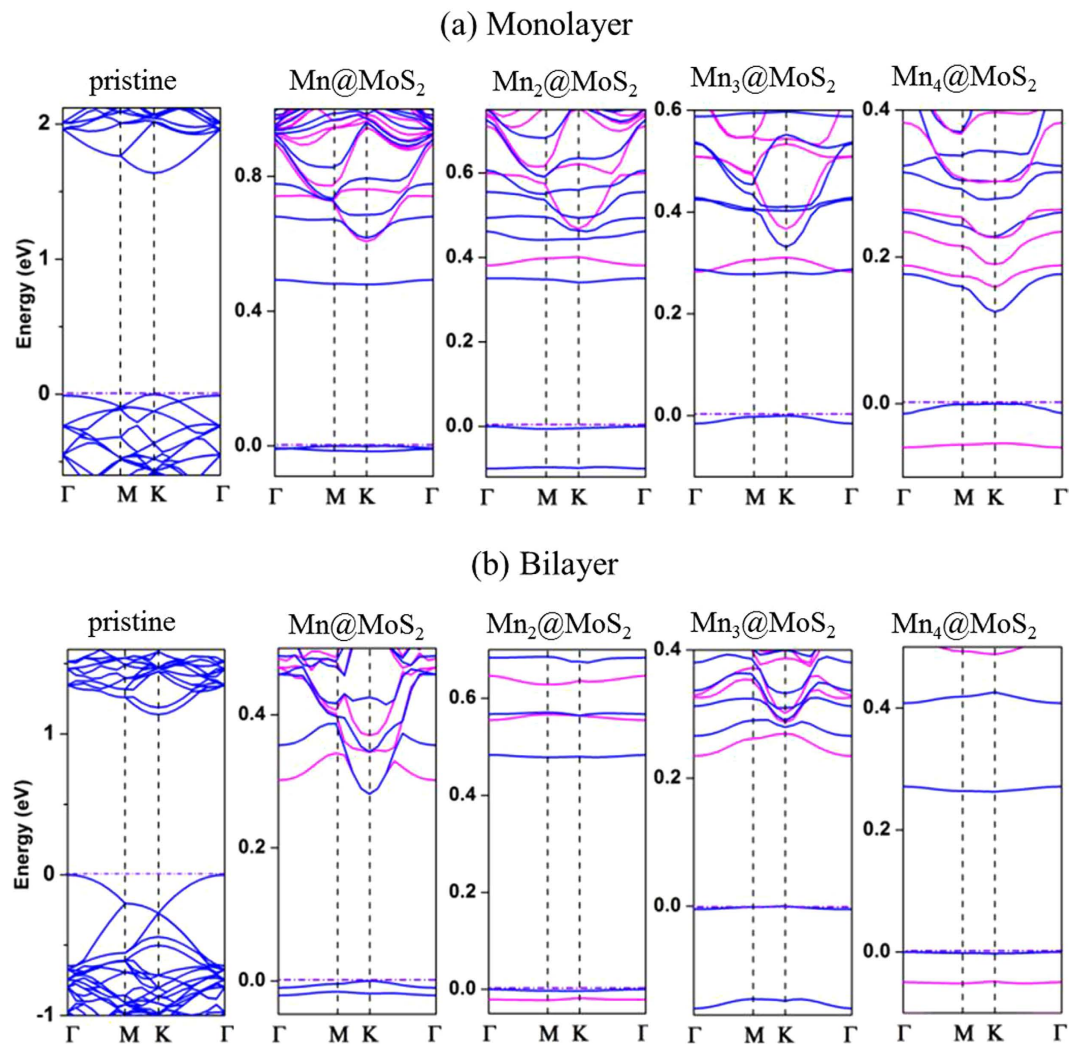
Figure 3. Spin-polarized band structures of the Mn_n adsorbed MoS_2 systems. (**a**) Band structures of the Mn_n@MoS_2 pizzas. (**b**) Band structures of the Mn_n@MoS_2 sandwiches. The blue and magenta lines represent the spin-up and spin-down components, respectively. The horizontal dash-dot lines indicate the Fermi level. The band structures of the pristine hosts are depicted at the very left column for comparison purpose.

purposes. In the monolayer, a direct bandgap was found to have energies of 1.69 eV and 1.89 eV in our GGA and Heyd-Scuseria-Ernzerhof (HSE06) calculations implemented in CASTEP package[45–47]. The values are in good agreement with previous studies[9,48–55]. Although GGA at the PBE level calculations typically underestimates this bandgap, there is no difference between the GGA and HSE06 evaluations of the bandgap types. As Fig. 3 shows, the embedment of the Mn_n clusters inserts additional defect states within the pristine MoS_2 bandgap. The valence band maximum (VBM) and conduction band minimum (CBM) are primary from the $3d$ orbitals of the Mn_n clusters. The partial density of states (PDOS) of Mn_n@MoS_2(M&B) in Fig. 4 clarifies theses defect states are from the Mn_n clusters near the VBM and the CBM. Compared with the pristine MoS_2 cases, Fermi energy shifts from the VBM towards the CBM with the increase of the Mn numbers. Figure 4 also shows that shapes of the total density of states for α electron (spin-up) and β electron (spin-down) near the Fermi energy are quite different in the contributions of the magnetism of the Mn_n@MoS_2. The bandgap of the pristine MoS_2 is evidently reduced due to the absorptions of small TM clusters. Such a reduction can significantly affect material optical and transport properties. From the values listed in Table 3, the bandgap of the 'pizzas' decreases gradually with the successive Mn atoms. However, odd-even oscillation emerges again in bilayer system similar to its magnetic properties.

As the Mn clusters are adsorbed on MoS_2, there is obvious hybridization between the atomic orbitals of the guest atom Mn and host atom S. We take the PDOS plots of Mo, S, and Mn atoms of the Mn_3@MoS_2(M) as an example (see Fig. 5) to explicate the hybridization. Several sharp peak superpositions originate from the PDOS for d orbital of Mn and p orbital of S in the S-Mn bond below the Fermi level. And the PDOS for Mo and S atoms in S-Mo bond close to the Mn cluster is quite different from these spectator Mo and S atoms far away the Mn cluster. Similar behavior is observed in all other Mn_n@MoS_2 systems.
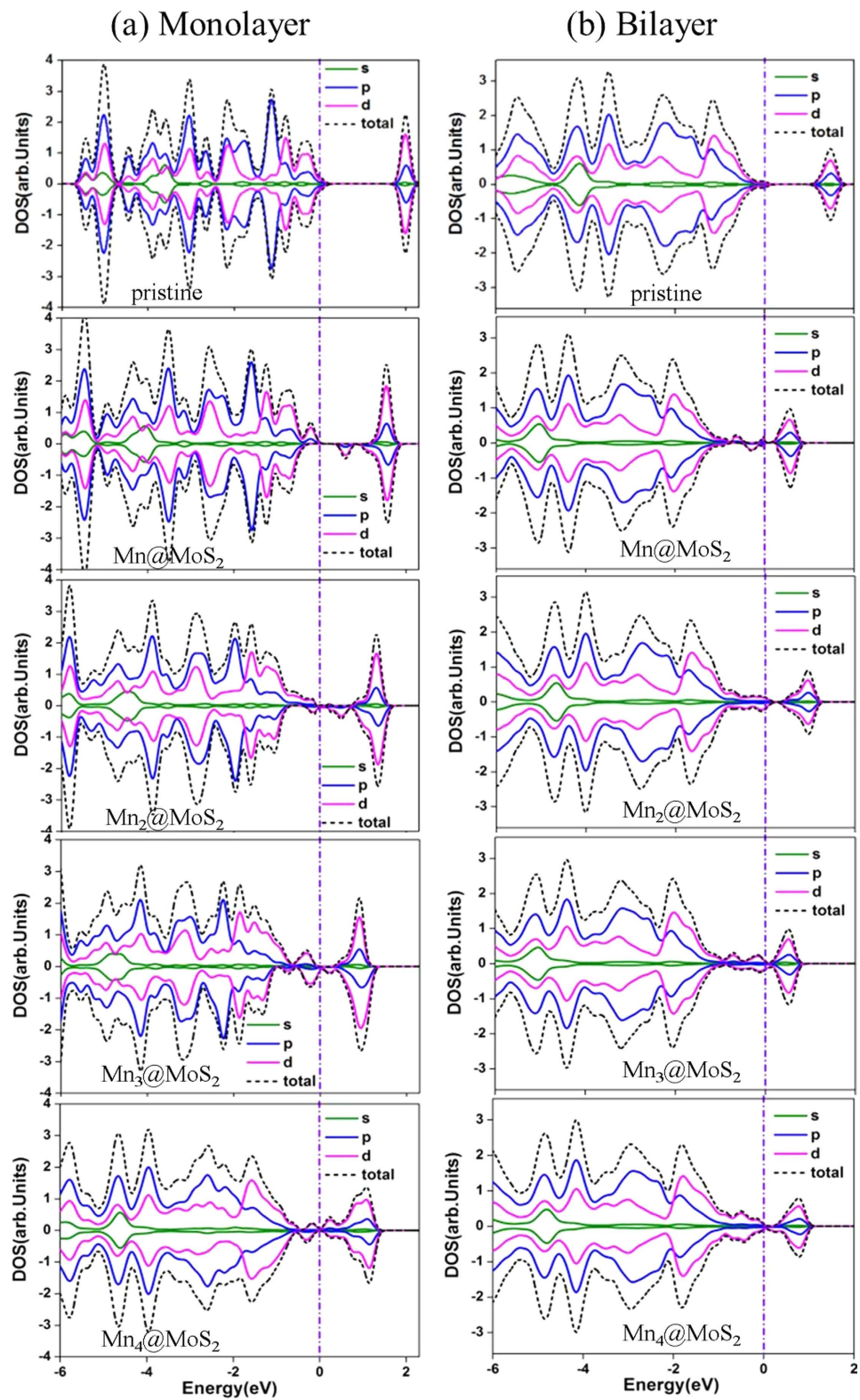
Figure 4. Electronic partial density of states (PDOS) of the Mn_n adsorbed MoS_2 systems. (**a**) The PDOS of spin-up (positive) and spin-down (negative) electrons of the $Mn_n@MoS_2$(M) pizzas. (**b**) The PDOS of spin-up (positive) and spin-down (negative) electrons of the $Mn_n@MoS_2$(B) sandwiches. The PDOS is obtained by Gaussian extension applied to the eigenvalues with a broadening width of 0.1 eV. The vertical dash-dot lines indicate the Fermi level.
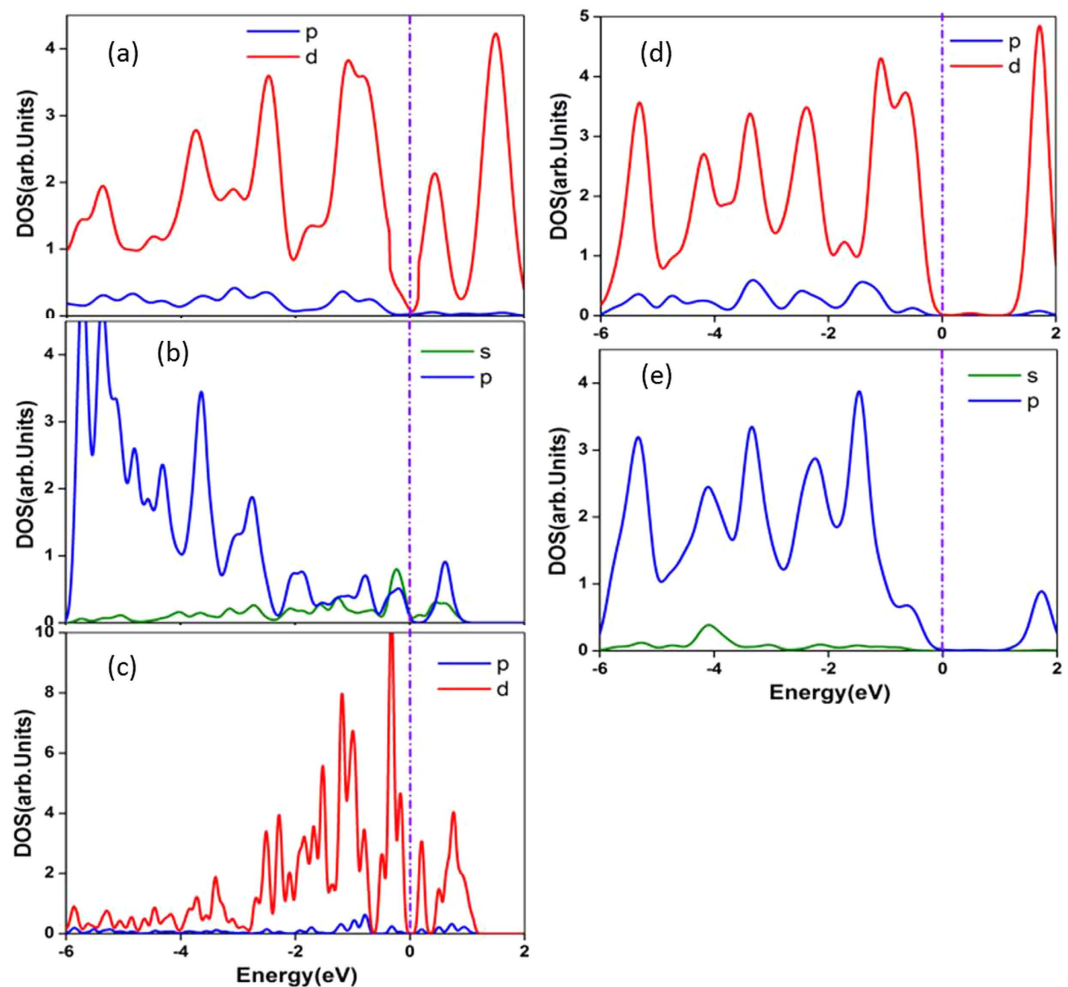
Figure 5. The PDOS of atoms in the Mn$_3$@MoS$_2$(M) complex. (**a**) Participator Mo atom near the Mn cluster. (**b**) Participator S atom contracting with Mn cluster. (**c**) Mn atom. (**d**) Spectator Mo atom away from the Mn cluster. (**e**) Spectator S atom away from Mn cluster. The illustration is the same as that in Fig. 4.

Types of bands can be switched through the present doping route. A transition from an indirect to a direct band-gap in pristine MoS$_2$ are found when the thickness is reduced from bilayer to a monolayer, in agreement with previous experimental reports[9,56] and theoretical results[57,58]. After the Mn$_n$ clusters were introduced to the host MoS$_2$ 'crusts', the Mn$_n$@MoS$_2$(M) pizza (n = 1,4) bandgaps keep direct as their host's. However, the bandgap turns to indirect when n = 2,3 as shown in Fig. 3a. Excitingly, in the case of the Mn$_1$@MoS$_2$(B) 'sandwich', the indirect bandgap of the bilayer host was switched to a direct bandgap. The CBM and VBM are both aligned at the κ point. Such a direct band structure is similar to the monolayer's ones, which have been considered as the crucial origin of the ILC unique material properties. The result indicates the bandgap of pristine MoS$_2$ can be operated from an indirect to direct or direct to indirect bandgap by adsorbing small TM clusters like Mn$_n$. This provides new opportunities for controlling electronic structures in nanoscale materials with novel optical behaviors.

Ranging from 0.053 to −0.215 and −0.32 to −1.715 au in the 'pizza' and 'sandwiches' systems, the net charge on the impurity Mn clusters clearly shows charge transfers between the 'toppings' and 'fillings', and the S atoms in the 'crusts' and 'slices'. This leads high stabilities of the 'pizza' and 'sandwiches' following the partially ionic-like bonding of the Mn−S interaction through the charge transfers. Except for the Mn$_1$@MoS$_2$(M), charge transfers occur from the S atoms to the Mn atoms resulting in negative charges of the Mn$_n$ clusters. For the Mn$_n$@MoS$_2$(B), increases of the net charge values on the Mn clusters were found, illustrating enhancements of the sandwiches structures as the successive add-on dopant. The charge transfers between the Mn clusters and host MoS$_2$ are one reason of the reducing magnetic moment of Mn$_n$@MoS$_2$ from the isolate Mn clusters, while strong hybridizations of the sulfur atoms in the MoS$_2$ with the d states of the Mn cluster atoms is counted as another.

Thermostabilities. The thermodynamic stability was tested by using the Born−Oppenheimer molecular dynamics simulation implemented in the DMOL3 code at room temperature (T = 300 K). A sample of the dynamic simulations is shown in Fig. 6 for the Mn$_3$@MoS$_2$(M) pizza case. It is clear that the relative potential energy remains unchanged within the selected time scale. The ground-state structure is stable at room temperature. Such a thermostability is in line with the experimental evidences of the Au adsorbed MoS$_2$ monolayer[59] and the latest results of the water intercalated organic counterpart of the graphene[35].
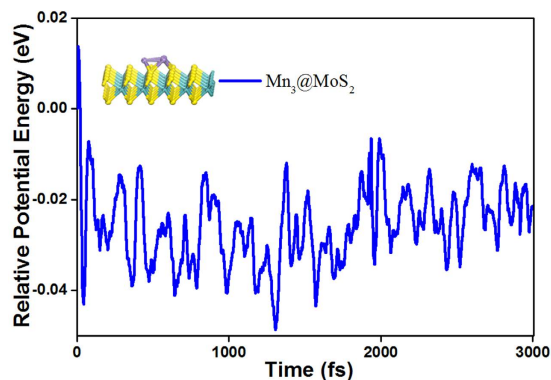
Figure 6. Relative potential energy (eV) of the lowest-energy structures Mn₃@MoS₂(M). The simulation time was set to 3 ps at a step interval of 1 fs in the molecular dynamics simulation.

In conclusion, we have presented a new strategy of tailoring the inorganic layered crystal to the magnetic semiconductors by introducing magnetic clusters as adsorbates. Geometric optimizations show that the small clusters prefer to follow the host alignments to enhance the complex stabilities. The magnetic and electronic structures were thoroughly explored. It is found that the system magnetic properties and electronic structures can be manipulated by careful selections of the 'pizza' and 'sandwich' recipes. Moreover, switches between the direct and indirect bandgaps of the adsorbed MoS_2 complexes were revealed. Benefiting from the uniqueness of the clusters and inorganic layered crystals, it is hoped that the present work will be served as a prototype in combinations of the cluster and layered crystal sciences, and boost their applications in the semiconducting scopes.

Methods

All calculations were performed by using the DMOL3 package[60,61]. Results from the present package were cross checked with the calculations from CASTEP package. A relativistic semi-core pseudopotential was employed for the spin-unrestricted calculations with double-numerical basis where d polarization functions (DNP) were included. Generalized gradient approximation in the Perdue−Burke−Ernzerhof (PBE) functional form was chosen[62]. The effect of van der Waals interactions was introduced explicitly through an empirical correction scheme proposed by Ortmann, Bechstedt, and Schmidt[63]. The quality of the self-consistent field (SCF) convergence tolerance was set as "fine". A convergence criterion of 1×10^{-5} hartree was applied on the total energy and electron density, 2×10^{-3} hartree/Å on the gradient, and 5×10^{-3} Å on lattice displacements. The 5×5 supercells were constructed from 75 atoms of 25 Mo atoms and 50 S atoms for the monolayer, and 150 atoms including 50 Mo atoms and 100 S atoms for the bilayer. A vacuum region of 25 Å was selected in the z-direction to exclude mirror interactions between neighboring images. The Brillouin Zone integrations were carried out on a $10 \times 10 \times 1$ Monkhorst−Pack k-points grad for the geometry optimizations, and a $15 \times 15 \times 1$ k-points grad for the band and density of states (DOS) properties. To elucidate system magnetic properties, we carried out a detailed calculation for each possible spin multiplicity (SM) ranging from 1 to 21 of the Mn_n (n = 1–4) adsorbed MoS_2 complexes.

References

1. Novoselov, K. S. *et al.* Electric field effect in atomically thin carbon films. *Science* **306,** 666–669 (2004).
2. Novoselov, K. S. *et al.* Two-dimensional gas of massless Dirac fermions in graphene. *Nature* **438,** 197–200 (2005).
3. Geim, A. K. Grapehen: status and prospects. *Science* **324,** 1530–1534 (2009).
4. Geim, A. K. & Grigorieva I. V. Van der Waals heterostructures. *Nature* **499,** 419–425 (2013).
5. Cohen, S. R. *et al.* The tribological behavior of type II textured MX₂ (M = Mo, W, X = S, Se) films. *Thin Solid Films* **324,** 190–197 (1998).
6. Furimsky, E. Role of MoS₂ and WS₂ in hydrodesulfuritation. *Catal. Rev.* **22,** 371–400 (1980).
7. Hinnemann, B. *et al.* Biomimetic hydrogen evolution: MoS₂ nanoparticles as catalyst for hydrogen evolution, *J. Am. Chem. Soc.* **127,** 5308–5309 (2005).
8. Splendiani, A. *et al.* Emerging photoluminescence in monolayer MoS₂. *Nano Lett.* **10,** 1271–1275 (2010).
9. Mak, K. F., Lee, C., Hone, J., Shan, J. & Heinz, T. F. Atomically thin MoS₂: A new direct-gap semiconductor. *Phys. Rev. Lett.* **105,** 136805 (2010).
10. Kim, S. *et al.* High-mobility and low-power thin-film transistors based on multilayer MoS₂ crystals. *Nat. Commun.* **3,** 1011 (2012).
11. Lopez-Sanchez, O., Lembke, D., Kayci, M., Radenovic, A. & Kis, A. Ultrasensitive photodetectors based on monolayer MoS₂. *Nat. Nanotechnol.* **8,** 497–501 (2013).
12. Kibsgaard, J., Chen, Z., Reinecke, B. N. & Jaramillo, T. F. Engineering the surface structure of MoS₂ to preferentially expose active edge sites for electrocatalysis. *Nat. Mater.* **11,** 863–869 (2012).
13. Butler, S. Z. *et al.* Progress, challenges, and opportunities in two-dimentsional materials beyond grapheme. *ACS Nano* **7,** 2898–2926 (2013).
14. Lee, Y. H. *et al.* Synthesis of large-area MoS₂ atomic layers with chemical vapor deposition. *Adv. Mater.* **24,** 2320–2325 (2012).
15. Ganatra, R. & Zhang, Q. Few-layer MoS₂: A promising layered semiconductor. *ACS Nano* **5,** 4074–4099 (2014).
16. Dietl, T., Ohno, H., Matsukura, F., Cibert, J. & Ferrand, D. Zener model description of ferromagnetism in zinc-blende magnetic semiconductors. *Science* **287,** 1019–1022 (2000).
17. Chambers, S. A. Ferromagnetism in doped thin-film oxide and nitride semiconductors and dielectrics. *Surf. Sci. Rep.* **61,** 345–381 (2006).

18. Yun, W. S. & Lee, J. D. Unexpected strong magnetism of Cu doped single-layer MoS_2 and its origin. *Phys. Chem. Chem. Phys*. **16,** 8990–8996 (2014).
19. Cheng, Y. C., Zhu, Z. Y., Mi, W. B., Guo Z. B. & Schwingenschlögl, U. Prediction of two-dimensional diluted magnetic semiconductors: Doped monlolyaer MoS_2 systems. *Phys. Rev. B* **87,** 100401 (2013).
20. Dolui, K., Rungger, I., Pemmaraju, D. C. & Sanvito, S. Possible doping strtegies for MoS_2 monolayers: An ab initio study. *Phys. Rev. B* **88,** 075420 (2013).
21. Komsa, H. P. *et al.* Two-dimensional transition metal dichalcogenides under electron irradiation: Defect production and doping. *Phys. Rev. Lett.* **109,** 035503 (2012).
22. Feng, N. *et al.* First principles prediction of the magnetic properties of $Fe-X_6$ (X = S, C, N, O, F) doped monolayer MoS_2. *Sci. Rep.* **4,** 3987 (2014).
23. Chen, Q., Ouyang, X., Yuan, S., Li, R. & Wang, J. Uniformly wetting deposition of Co atoms on MoS_2 monolayer: A promising two-dimensional robust half-metallic ferromagnet. *ACS Appl. Mater. Inter.* **6,** 16835−16840 (2014).
24. Shu, H., Luo, P., Liang, P., Cao, D. & Chen, X. Layer-dependent dopant stability and magnetic exchange coupling of iron-doped MoS_2 nanosheets. *ACS Appl. Mater. Inter.* **7,** 7534–7541 (2015).
25. Park, J., Privman, V. & Matijević, E. Model of formation of monodispersed colloid. *J. Phys. Chem. B* **105,** 11630–11635 (2001).
26. Lu, A. H., Salabas, E. L. & Schüth, F. Magnetic nanoparticles: synthesis, protection, functionalization, and application. *Angew. Chem. Int. Edit.* **46,** 1222–1244 (2007).
27. Cheng, F., Chen, J. & Gou, X. MoS_2-Ni nanocomposites as catalysts for hdrodesulfurization of thiophene and thiophene derivatives. *Adv. Mat*er **18,** 2561–2564 (2006).
28. Sarkar, D. *et al.* Functionalization of transition metal dichalcogenides with metallic nanoparticles: Implications for doping and gas-sensing. *Nano Lett.* **15,** 2852–2862 (2015).
29. Cao, W. *et al.* Gold nanoparticles on MoS_2 layered crystal flakes. *Mater. Chem. Phys.* **158,** 89–95 (2015).
30. Kroto, H. W., Heath, J. R., O'Brien, S. C., Curl, R. F. & Smalley, R. E. C60: Buckminsterfullerene. *Nature* **318,** 162–163 (1985).
31. Pyykkö, P. Structural properties: Magic nanoclusters of gold. *Nat. Nanotechnol.* **2,** 273–274 (2007).
32. Liu, X., Wang, C. Z., Lin, H. Q. & Ho, K. M. Magnetic moment enhancement for Mn_7 cluster on graphene. *J. Phys. Chem. C* **118,** 19123–19128 (2014).
33. Sahoo, S., Islam, M. F. & Khanna, S. N. Using graphene to control magnetic anisotropy and interaction between supported clusters. *New J. Phys.* **17,** 053052 (2015).
34. Wang, G. *et al.* Nickel cluster growth on defect sites of graphene: A computational study. *Angew. Chem. Int. Edit.* **52,** 14237–14241 (2013).
35. Algara-Siller, G. *et al.* Square ice in graphene nanocapillaries. *Nature* **519,** 443–445 (2015).
36. Zhang, M. *et al.* First-principles investigations of chirality in trimetallic alloy clusters: $AlMnAu_n$ (n = 1–7). *J. Phys. Chem. A* **119,** 3458–3470 (2015).
37. Bobadova-Parvanova, P., Jackson, K. A., Srinivas, S. & Horoi, M. Emergence of antiferromagnetic ordering in Mn clusters. *Phys. Rev. A* **67,** 061202 (2003).
38. Rigo, V. A., Miwa, R. H., da Silva, A. J. R. & Fazzio, A. Mn dimers on graphene nanoribbons: An ab initio study. *J. Appl. Phys.* **109,** 053715 (2011).
39. Kabir, M., Mookerjee, A. & Kanhere, D. G. Structure, electronic properties, and magnetic transition in manganese clusters. *Phys. Rev. B* **73,** 224439 (2006).
40. Longo, R. C., Noya, E. G. & Gallego, L. J. Fully unconstrained density-functional study of the structures and magnetic moments of small Mn_n clusters (n = 2–7). *Phys. Rev. B* **72,** 174409 (2005).
41. Gutsev, G. L., Mochena, M. D. & Bauschlicher, Jr. C. W. Structure and properties of Mn_n, Mn_n^-, and Mn_n^+ clusters (n = 3−10). *J. Phys. Chem. A* **110,** 9758–9766 (2006).
42. Ataca, C. & Ciraci, S. Functionalization of single-layer MoS_2 honeycomb structures. *J. Phys. Chem. C* **115,** 13303–13311 (2011).
43. Ramasubramaniam, A. & Naveh, D. Mn-doped monolayer MoS_2: An atomically thin dilute magnetic semiconductor. *Phys. Rev. B* **87,** 195201 (2013).
44. He, J., Wu, K., Sa, R., Li, Q. & Wei, Y. Magnetic properties of nonmetal atoms adsorbed MoS_2 monolayers. *Appl. Phys. Lett.* **96,** 082504 (2010).
45. Bu, H. *et al.* Isoelectronic doping of graphdiyne with boron and nitrogen: Stable configurations and band gap modification. *J. Phys. Chem. A* **116,** 3934 (2012).
46. Zhao, M., Dong, W. & Wang, A. Two-dimensional carbon topological insulators superior to graphene. *Sci. Rep.* **3,** 3532 (2013).
47. Huang, H., Duan, W. & Liu, Z. The existence/absence of Dirac cones in graphynes. *New J. Phys.* **15,** 023004 (2013).
48. Zhou, Y. G., Su, Q. L., Wang, Z. G., Deng, H. Q. & Zu, X. T. Controlling magnetism of MoS_2 sheets by embedding transition-metal atoms and applying strain. *Phys. Chem. Chem. Phys.* **15,** 18464–18470 (2013).
49. Terrones, H., López-Urías, F. & Terrones, M. Novel hetero-layered materials with tunable direct band gaps by sandwiching different metal disulfides and diselenides. *Sci. Rep.* **3,** 1549 (2013).
50. Johari, P. & Shenoy, V. B. Tuning the electronic properties of semiconducting transition metal dichalcogenides by applying mechanical strains. *ACS Nano* **6,** 5449–5456 (2012).
51. Yun, W. S., Han, S. W., Hong, S. C., Kim, I. G. & Lee, J. D. Thickness and strain effects on electronic structures of transition metal dichalcogenides: $2H-MX_2$ semiconductors (M = Mo, W; X = S, Se, Te). *Phys. Rev. B* **85,** 033305 (2012).
52. Scalise, E., Houssa, M., Pourtois, G., Afanas'ev, V. & Stesmans, A. Strain-induced semiconductor to metal transition in the two-dimensional honeycomb structure of MoS_2. *Nano Res.* **5,** 43–48 (2012).
53. Han, S. W. *et al.* Band-gap transition induced by interlayer van der Waals interaction in MoS_2. *Phys. Rev. B* **84,** 045409 (2011).
54. Kuc, A., Zibouche, N. & Heine, T. Influence of quantum confinement on the electronic structure of the transition metal sulfide TS_2. *Phys. Rev. B* **83,** 245213 (2011).
55. Ramasubramaniam, A., Naveh, D. & Towe, E. Tunable band gaps in bilayer transition-metal dichalcogenides. *Phys. Rev. B* **84,** 205325 (2011).
56. Splendiani, A. *et al.* Emerging photoluminescence in monolayer MoS_2. *Nano Lett.* **10,** 1271–1275 (2010).
57. Ellis, J. K., Lucero, M. J. & Scuseria, G. E. The indirect to direct band gap transition in multilayered MoS_2 as predicted by screened hybrid density functional theory. *Appl. Phys. Lett.* **99,** 261908 (2011).
58. Cheiwchanchamnangij, T. & Lambrecht, W. R. L. Quasiparticle band structure calculation of monolayer, bilayer, and bulk MoS_2. *Phys. Rev. B* **85,** 205302 (2012).
59. Lin, Y. C. *et al.* Properties of individual dopant atoms in single-layer MoS_2: Atomic structure, migration, and enhanced reactivity. *Adv. Mater.* **26,** 2857–2861 (2014).
60. Delley, B. An all-electron numerical method for solving the local density functional for polyatomic molecules. *J. Chem. Phys.* **92,** 508–517 (1990).
61. Delley, B. From molecules to solids with the DMol3 approach. *J. Chem. Phys.* **113,** 7756–7764 (2000).
62. Perdew, J. P., Burke, K. & Ernzerhof, M. Generalized gradient approximation made simple. *Phys. Rev. Lett.* **77,** 3865–3868 (1996).
63. Ortmann, F., Bechstedt, F. & Schmidt, W. G. Semiempirical van der Waals correction to the density functional description of solids and molecular structures. *Phys. Rev. B* **73,** 205101 (2006).

Acknowledgements

Author Contributions

The project was initiated by W.C. and conceived by W.C. and M.Z. M.Z. conducted the calculations. Z.H., X.W., H.Z., T.L., Z.W. and Y.L. participated in the calculations and structural optimizations. The article was written by M.Z. and W.C. All authors have read and commented on the manuscripts.

Additional Information

Supplementary information accompanies this paper at http://www.nature.com/srep

Competing financial interests: The authors declare no competing financial interests.

How to cite this article: Zhang, M. *et al.* Magnetic MoS$_2$ pizzas and sandwiches with Mn$_n$ (n=1–4) cluster toppings and fillings: A first-principles investigation. *Sci. Rep.* **6**, 19504; doi: 10.1038/srep19504 (2016).